Supporting Information

The effect of centred versus offset interpenetration on C$_2$H$_2$ sorption in hybrid ultramicroporous materials

Alankriti Bajpai,[a,‡] Daniel O'Nolan,[a,‡] David G. Madden,[a,‡] Kai-Jie Chen,[a] Tony Pham,[b] Amrit Kumar,[a] Matteo Lusi,[a] John J. Perry IV,[a] Brian Space[b] and Michael J. Zaworotko[a]*

[a]Department of Chemical Sciences and Bernal Institute, University of Limerick, Republic of Ireland
[b]Department of Chemistry, University of South Florida, 4202 East Fowler Avenue, Tampa, Florida, 33620, U.S.A

‡ These authors contributed equally to this work.
* Corresponding Author, xtal@ul.ie

Table of Contents

Experimental Procedures

All reagents and solvents were purchased from Sigma-Aldrich and used as received. 1,2-Bis(4-pyridyl)acetylene (ligand **2**) and 1,2-bis(4-pyridyl)benzene (ligand **4**) were synthesised following previously described Pd^0-catalysed cross coupling protocols.[1] $[Cu(TiF_6)]\cdot xH_2O$ was prepared as previously reported.[2] **SIFSIX-2-Cu-i** and **TIFSIX-2-Cu-i** were synthesised based on our previous report.[3]

Preparation of {[Cu(1,4-Bis(4-pyridyl)benzene)$_2$(TiF$_6$)]$_n$} (TIFSIX-4-Cu-i). A blank layer of MeOH/ethylene glycol (2 mL; 1:1 *v/v*) was carefully layered over a solution of ammonium hexafluorotitanate (0.01 mmol) and copper nitrate trihydrate (0.01 mmol) in 3 mL of water/ethylene glycol (1:2, *v/v*) mixture. Over this was layered a solution of ligand **4** in 2 mL of MeOH (5 mg, 0.02 mmol). Violet needles were obtained after two weeks.

The sample was activated by solvent exchange *via* Soxhlet extraction using MeOH followed by heating at 70 °C *in vacuo* for 12 h for gas sorption measurements.

Powder X-ray Diffraction (PXRD). Qualitative diffraction patterns were collected on a PANalytical Empyrean™ diffractometer mounted with a PIXcel^{3D} detector under Bragg-Brentano geometry in continuous scanning mode. An Empyrean Cu LFF (long fine-focus) HR (9430 033 7310x) tube was used at 40 kV and 40 mA and CuKα radiation (λ = 1.540598 Å). Incident beam optics was composed of a 1/8° divergence slit and a 1/4° anti-scatter slit, a 10 mm fixed incident beam mask and a Soller slit (0.04 rad). Divergent beam optics was composed of a P7.5 anti-scatter slit, a Soller slit (0.04 rad), and a Ni-β filter.

Single Crystal X-ray Diffraction (SXRD). X-ray diffraction data for as-synthesised **TIFSIX-4-Cu-i** was collected on a Bruker D8 Quest Diffractometer equipped with a microfocus Cu source and a Photon detector at 100(2) K under N_2 flow. Data were corrected for absorption using empirical methods (SADABS) based upon symmetry-equivalent reflections combined with measurements at different azimuthal angles. Crystal structures were solved and refined against all F^2 values using the SHELX suite of programs interfaced with X-SEED.[4] All non-hydrogen atoms were refined anisotropically and hydrogen atoms placed in calculated positions refined using idealised geometries (riding model) and assigned fixed isotropic displacement parameters.

Variable Temperature Powder X-ray Diffraction (VT-PXRD). The variable temperature PXRD (VT-PXRD) were collected on Philips X'Pert PRO MPD equipped with a Cu-Kα source (λ = 1.540598 Å) under N_2 atmosphere between 25 °C and 200 °C.

Synchrotron X-ray Powder Diffraction (PXRD). The structure model for the activated sample of **TIFSIX-4-Cu-i** (**TIFSIX-4-Cu-i-β**) was obtained from the PXRD data collected at ambient pressure and 293 K on the beamline i11 at the Diamond Light Source[5] (λ = 0.826041(10) Å and zero point = -0.001217(3)) using a 2 s scan with positional scanning detectors. The diffraction peaks were indexed with DICVOL6.[6] The unit cell space group was determined by statistical analysis of the systematic absences. The intensities extraction was performed by Pawley refinement: Pawley R_{exp} 5.09%; χ^2 96.47. Structure solutions by simulated annealing and rigid-body constrains using the CCDC DASH[7] software. The initial conformation of the rigid-body model was derived from the single crystal data of as-synthesised **TIFSIX-4-Cu-i** (**TIFSIX-4-Cu-i-α**). Rietveld refinement was performed on a structure model that excluded H atoms. Hydrogen atoms were placed in calculated positions and refined using idealised geometries (riding model). All atoms were assigned fixed isotropic displacement parameters. Further Rietveld refinement was completed with GSAS-II.[8]

Rietveld Refinment Summary (GSAS .lst file):

```
Restraint data statistics: No restraints used
Powder data statistics          Fitted     -Bknd       pFree          Average

Bank Ndata Sum(w*d**2) wRp   Rp   wRp   Rp   wRp   Rp  Npfree DWd Integral
Hstgm  1 PXC   1 24999 5.87172E+05 0.4016 0.3212 0.9158 0.3559 0.0000 0.0000   0  0.039  0.583
Powder totals     24999 5.87172E+05 0.4016 0.3212 0.9158 0.3559 0.0000 0.0000   0  0.039

No serial correlation in fit at 90% confidence for 1.962 < DWd < 2.038
Cycle  24 There were  24999 observations.
Total before-cycle CHI**2 (offset/sig) = 5.8717E+05 ( 2.5147E+03)
Reduced CHI**2 = 23.50    for   10 variables
After matrix normalisation and Marquardt modification:

  1 Columns of the    10 Column matrix are 0.0
Full matrix recip. condition value & -log10 =  0.4112E-01    1.39
      Variable    1HSCL was not refined

The value of the determinant is  5.2642*10.0**(  -2)
Calculated unit cell formula weight:    0.000, density:  0.000gm/cm**3

Histogram scale factors:
Histogram:  1 PXC
Scale   :     1.00000
Sigmas  :     0.00000
Shift/esd:     0.00
Histogram scale factor sum(shift/error)**2 :     0.00
```

```
 Profile coefficients for histogram no.  1 and for phase no.  1:
Coeff. :   GU      GV      GW      LX      LY      trns    asym    shft    GP      stec
Value   : 5.937E+02 3.263E+01 1.726E+00 1.001E+00 9.055E+00 0.000E+00 8.642E-02 0.000E+00
0.000E+00 0.000E+00
Sigmas :                         7.888E-01
Shift/esd:                        8.00
Coeff. :   ptec    sfec    L11     L22     L33     L12     L13     L23
Value   : 0.000E+00 0.000E+00 0.000E+00 0.000E+00 0.000E+00 0.000E+00 0.000E+00 0.000E+00
Sigmas :
Shift/esd:
Profile coef. sum(shift/error)**2 :   64.08
Background coefficients for histogram no.  1:
Param. :      1        2        3        4        5        6
Coeff. : 4.183231E+01 -2.271813E+01 -1.223235E+01 2.746579E+01 -1.906443E+01 8.696457E+00
Sigmas : 2.122892E-01 2.878751E-01 2.586656E-01 2.551547E-01 2.482105E-01 2.460021E-01
Shift/esd:    -36.98     -26.40     22.07     29.94     0.87     -15.17
Param. :      7        8
Coeff. : 1.981249E-01 6.467021E+00
Sigmas : 2.504787E-01 2.490109E-01
Shift/esd:    1.77     12.01
Background coef. sum(shift/error)**2 :  3826.30
CPU times for matrix build    0.27 sec; matrix inversion    0.00 sec
Final variable sum((shift/esd)**2) for cycle  24:   3890.37 Time:   0.27 sec
```

Thermogravimetric Analysis (TGA). Thermogravimetric analyses were measured using a TA Q50 V20.13 Build 39 in High Resolution Dynamic mode with a sensitivity of 1.0, a resolution of 4.0, and a temperature ramp of 20 °C/min from ambient temperature up to 500 °C under a 60 mL/min flow rate of N_2 gas. Approximately 15 mg of sample were loaded onto platinum pans.

Gas Sorption Measurements. Adsorption experiments (up to 1 bar) for different pure gases were performed on Micromeritics TriStar II PLUS and Micromeritics 3-Flex surface area and pore size analyser using ultra-high purity grade N_2 (99.999%), C_2H_2 (99.99%), and C_2H_4 (99.99%) as-received from BOC gases. As-synthesised samples were activated by solvent-exchange using MeCN (**SIFSIX-2-Cu-i** and **TIFSIX-2-Cu-i**) or MeOH (**TIFSIX-4-Cu-i**) for up to 7 d and subsequently degassed at rt under high vacuum (<0.5 mmHg) for 24-48 h on a Smart VacPrep instrument prior to the analysis. The 273 K and 298 K bath temperatures were controlled using a Julabo ME (v.2) recirculating control system filled with a mixture of ethylene glycol and water. Low temperatures of 77 K and 195 K were maintained in a 4 L Dewar flask filled with liquid N_2 and dry ice/acetone slurry, respectively. N_2 adsorption isotherms at 77 K were used to determine Brunauer-Emmett-Teller (BET) surface using Micromeritics Microactive software. Approximately 100-200 mg of activated sample was used for all adsorption measurements. Low pressure C_2H_2 and C_2H_4 measurements were performed on the Micromeritics 3 Flex surface area and pore size analyser at 273 K, 283 K, and 298 K. (**Figures S8-S13**, **S19-S20**).

Dynamic Mixed Gas Breakthrough Studies. In a typical experiment, *ca.* 250 mg of finely ground activated sample was placed in a quartz tube ($\emptyset$ = 8 mm) to form a fixed-bed held in place using quartz wool. Each sample was heated to 60 °C under a dry helium flow to remove atmospheric contaminants. Upon cooling, a C_2H_2/C_2H_4 mixture (1/99, *v/v*) was passed over the packed bed with a total flow rate of 10 cm^3/min at 298 K. The outlet gas concentration was continuously monitored using a Hiden HPR-20 QIC evolved gas analysis mass spectrometer (EGA-MS).

Upon complete breakthrough and saturation of the packed bed adsorbent, the mixed gas inflow is switched off and samples regenerated by purging dry helium followed by heating to 60 °C. **TIFSIX-14-Cu-i** was regenerated in the absence of heat due to its lower thermal stability. Upon cooling of sample to 298 K, C_2H_2/C_2H_4 mixture (1/99, *v/v*) was again introduced for the next cycle of breakthrough.

Accelerated Stability Protocol. Approved as a unified testing condition by International Conference of Harmonization (ICH), the accelerated stability protocol takes into account all possible storage conditions from different regions around the globe and consists of long-term, intermediate and accelerated storage conditions valid for the USA, EU and Japan. Verified by Arrhenius equation, accelerated stability conditions mimic an acceleration of the storage at ambient conditions, and accelerated stability testing for 6 months is equivalent to two years of long-term storage conditions. In an archetypal experiment, pristine activated sample of the adsorbent was subjected to elevated relative humidity and temperature. To achieve 75% relative humidity at 40 °C, saturated aq. NaCl solution is placed in a desiccator stored at 40 °C. Samples were placed in a separate, open glass vials and placed in this desiccator. Aliquots were removed for analysis (PXRD, TGA and gas adsorption) after 1, 7 and 14 d.

Powder X-ray Diffraction Data
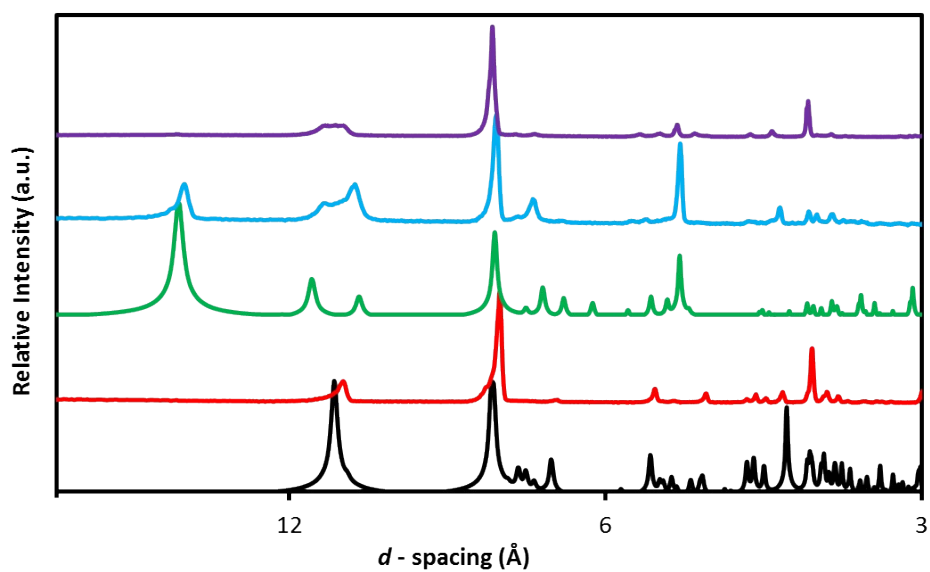
Figure S1. Powder X-ray diffractograms of **TIFSIX-4-Cu-i** under various conditions. As-synthesised **TIFSIX-4-Cu-i** calculated (black), **TIFSIX-4-Cu-i-α** experimental (red), **TIFSIX-4-Cu-i-β** calculated (green), activated **TIFSIX-4-Cu-i** (blue), **TIFSIX-4-Cu-i** soaked in methanol (purple).

Single Crystal X-ray Diffraction Data

Table S1. Crystallographic data for as-synthesised **TIFSIX-4-Cu-i** (**TIFSIX-4-Cu-i-α**).

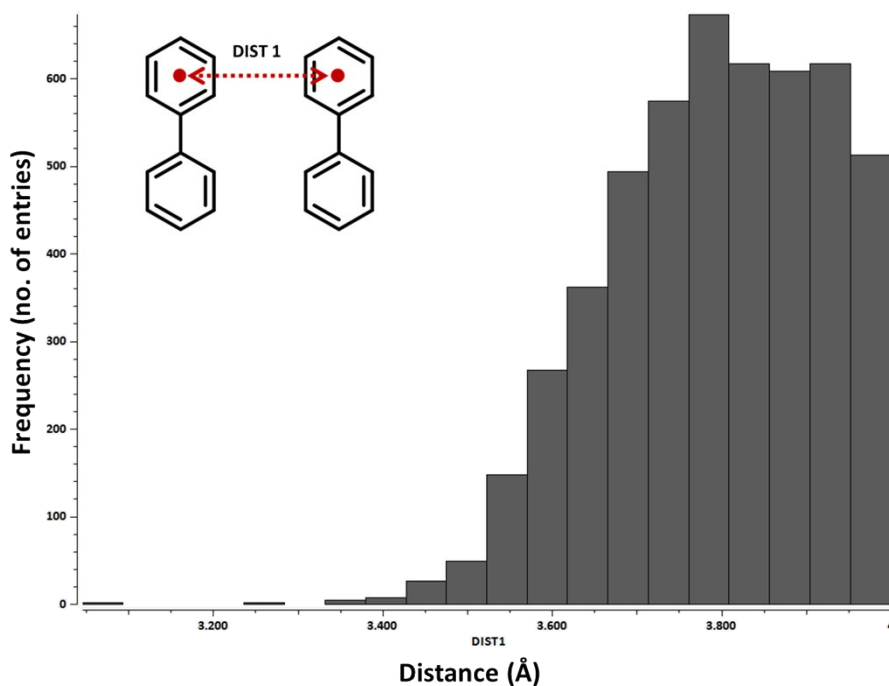|	TIFSIX-4-Cu-i-α
Molecular formula	$C_{18}H_{20}N_2O_2CuTiF_6$
Formula weight	521.77
Temperature (K)	100(2)
Wavelength (Å)	1.54178
Crystal system	monoclinic
Space group	$C2/c$ (no. 15)
a (Å)	17.6291(8)
b (Å)	15.4159(7)
c (Å)	16.1386(7)
α (°)	90
β (°)	119.600(2)
γ (°)	90
Volume (Å^3)	3813.6(3)
Z	4
Calculated density (g/cm^3)	1.425
Absorption coefficient (mm^{-1})	3.097
F(000)	1684
Data/restraints/parameters	1986/0/246
Goodness-of-fit on F^2	1.167
Final R indices [I>2σ(I)]	0.1045 (wR2 = 0.2968)
R indices (all data)	0.1063 (wR2 = 0.2975)

Crystal Structure Description

TIFSIX-4-Cu-i crystallises in the monoclinic space group $C2/c$ with 0.5 Cu^{2+} and Ti^{2+} ions each, three F atoms, two crystallographically independent molecules of **4** each with 0.5 occupancy, and two molecules of MeOH comprising the asymmetric unit (Table S2). The hexacoordinated Cu^{2+} center serves as an octahedral 6-c node; four pyridyl groups of **4** coordinate equatorially to form a square lattice (**sql**) network. The Cu^{2+} nodes coordinate axially to F atoms from TiF$_6^{2-}$ anions pillaring the **sql** nets into the observed primitive cubic (**pcu**) network. Notably, the inorganic pillars, unlike in all of the previously reported **MFSIX** structures, are found to be bent ($\angle_{Ti-F-Cu}$ = 160.2°), Figure S1d. 2-Fold centred interpenetration is observed such that the central benzene rings of **4** interact closely via π-π stacking (*ca.* 3.62 Å). The torsion angles of pyridyl rings with respect to central benzene ring are found to be 57.9 and 41.4°. The mean values of the torsion angles reported for **4** in Cambridge Structural Database (CSD)[9,10] are 27.8° and 28.6°. Slight increase in the torsion angle is presumably to facilitate better π-π stacking interaction between the two interpenetrated networks. Two MeOH

8

molecules are located in the 1D channels and are found to be H-bonded to the equatorial F atoms of the TiF_6^{2-} moiety ($d_{O-H\cdots F}$ = 2.23 Å, $D_{O\cdots F}$ = 2.95 Å, $\angle_{O-H\cdots F}$ = 144.0°). The purity of as-synthesised and activated bulk samples was validated by powder X-ray diffraction (PXRD; Figure S1). Thermogravimetric analysis (TGA) reveals that solvent molecules are lost well before the disintegration of network (*ca*. 250-270 °C). PXRD data collected before and after desolvation at 60 °C suggest a phase transformation (Figure S1). Synchrotron PXRD data collected under vacuum on a desolvated sample of **TIFSIX-4-Cu-i-α**, i.e. **TIFSIX-4-Cu-i-β**, revealed a change in space group (from *C2/c* to *Cmcm*) and mode of interpenetration (from centred to offset), Figure S2. The two interpenetrated networks in **TIFSIX-4-Cu-i-β** are offset leading to formation of three distinct pores (Figure S2e). The inorganic pillars in **TIFSIX-4-Cu-i-β** are found to be linear, Figure S2h. Figure S3 shows the statistical distribution of π-π stacking distances between aryl rings for the structures reported in the CSD. The distance between the linkers **4** belonging to the two interpenetrated networks in activated **TIFSIX-4-Cu-i** are 3.864(1) Å indicating presence of π-π stacking interactions between the two interpenetrated networks. VT-PXRD revealed the phase transformation to be associated with the loss of MeOH (Figure S4). **TIFSIX-4-Cu-i-β** reverted to **TIFSIX-4-Cu-i-α** only on soaking in MeOH indicating solvent-induced breathing.
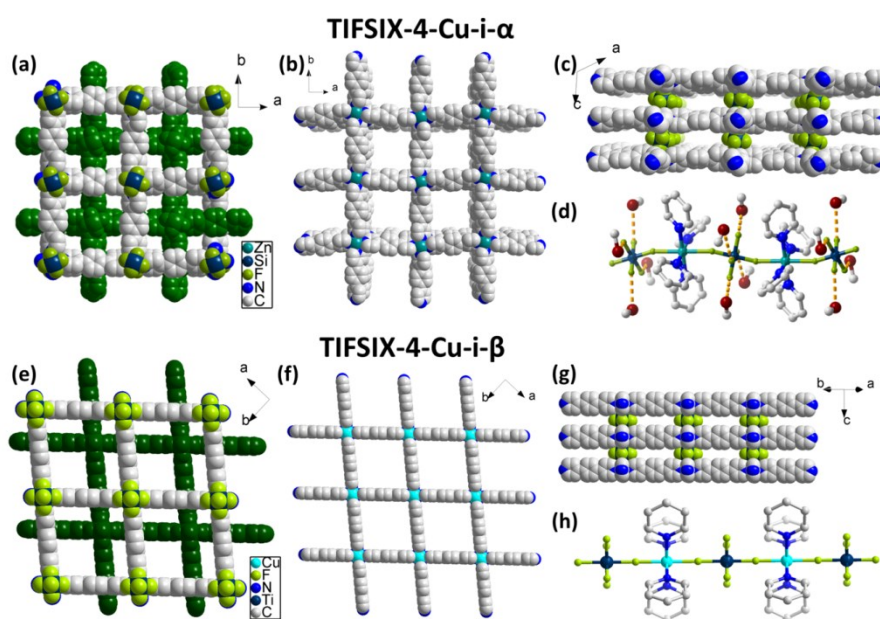

Figure S2. Comparison of the crystal structures of as-synthesised **TIFSIX-4-Cu-i-α** and desolvated **TIFSIX-4-Cu-i-β:** (a,e) Crystal packing diagrams depicting centred and offset 2-fold interpenetration in **TIFSIX-4-Cu-i-α** and **TIFSIX-4-Cu-i-β**, respectively. One of the **pcu** nets is shown in green. (b,f) 2D sheets are formed by the coordination of Cu^{2+} ions to four molecules of ligand **4**. (c,g) TiF_6^{2-} inorganic pillars cross-link that the 2D layers into 3D network with **pcu** topology. (d) The inorganic pillars exhibit a tilted orientation with the equatorial fluorine atoms H-bonded to MeOH molecules, which occupy the void spaces. (h) The inorganic pillars are linear in **TIFSIX-4-Cu-i-β**. Hydrogen atoms have been omitted for clarity.

**Figure S3**. Histogram showing the statistical distribution of π-π stacking distances (Å) between aryl rings. The distance between the linkers **4** belonging to the two interpenetrated networks in **TIFSIX-4-Cu-i-β** is 3.864(1) Å.

Variable-Temperature Powder X-ray Diffraction Data
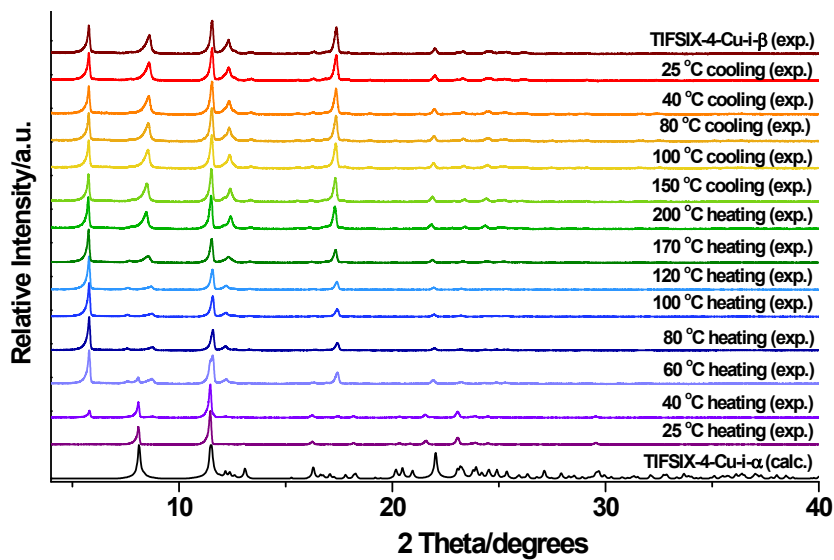
Figure S4. *In-situ* variable-temperature PXRD (VT-PXRD) of **TIFSIX-4-Cu-i** under N_2 atmosphere.
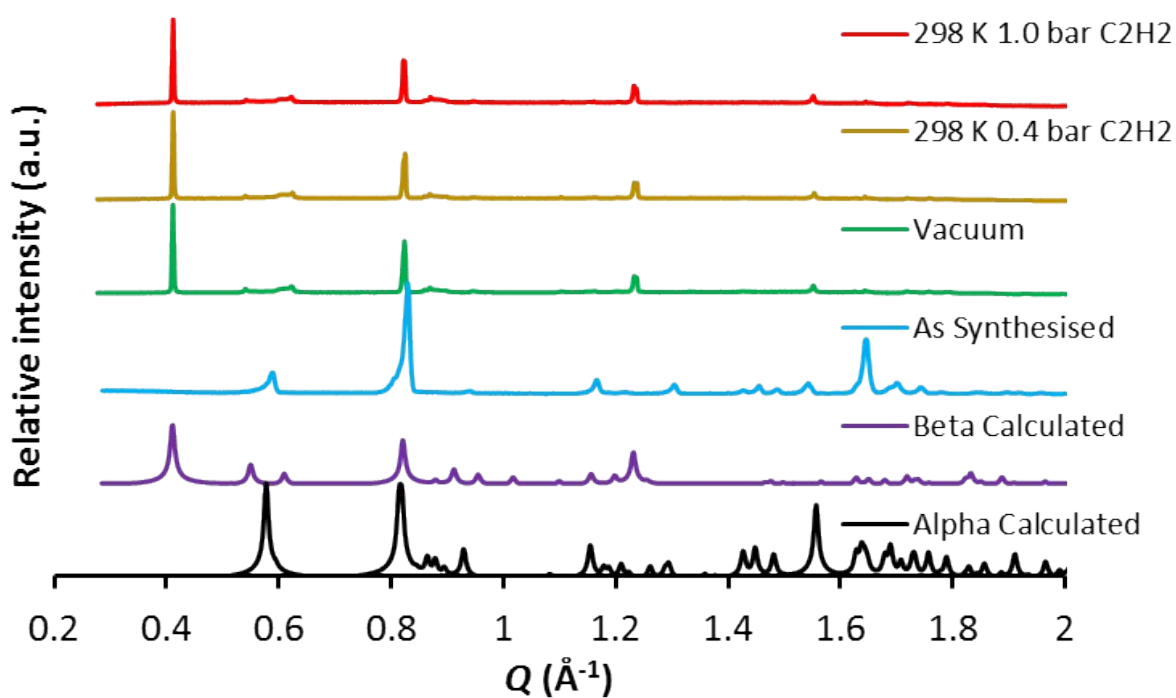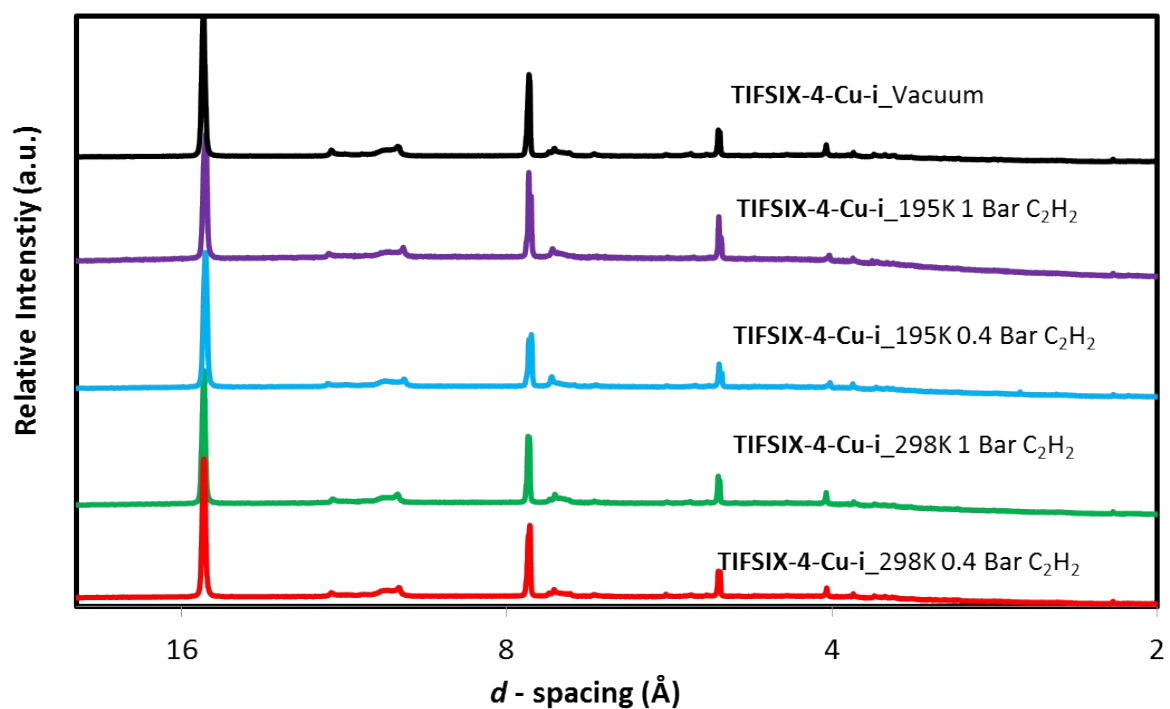
Synchrotron X-ray Powder Diffraction
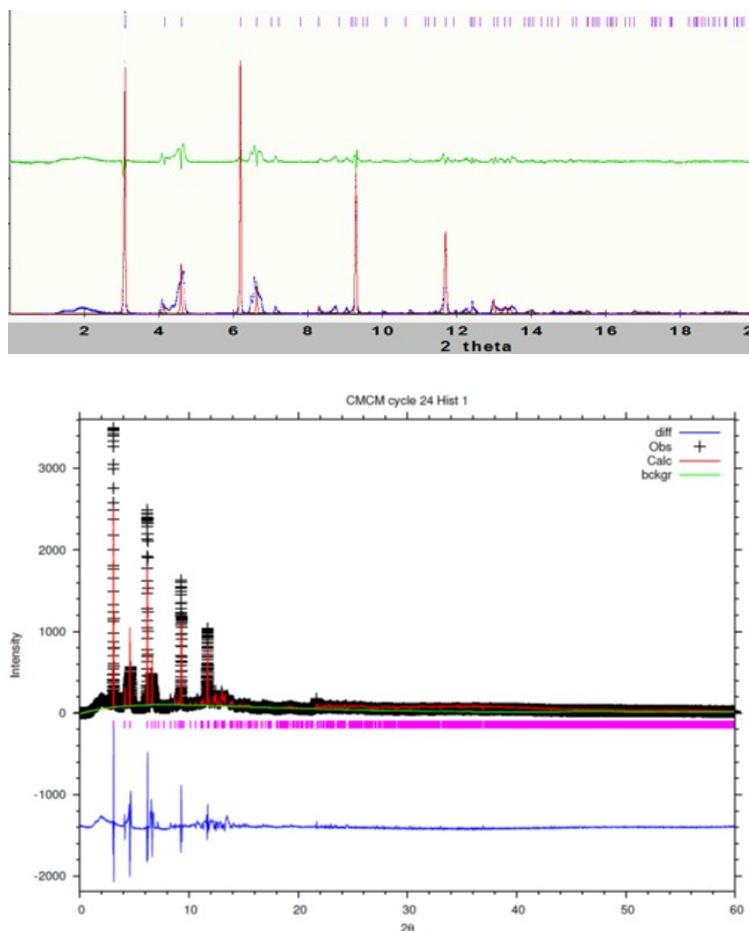
Figure S5. Difference plot of Pawley (top) and Rietveld refinement fitting of synchrotron X-ray powder diffraction data for activated **TIFSIX-4-Cu-i** (**TIFSIX-4-Cu-i-β).**

Table S2. Crystallographic data for synchrotron powder X-ray diffraction refinement of activated **TIFSIX-4-Cu-i** (**TIFSIX-4-Cu-i-β**) and laboratory X-ray diffraction refinement of **TIFSIX-14-Cu-i**.

Compound	TIFSIX-4-Cu-i-β	
Formula	$C_{32}H_{24}CuF_6N_4Ti$	
Bravais lattice	Orthorhombic	
Space group	*C mcm*	
	$a = 22.924(28)$ Å	$\alpha = 90°$
Unit cell parameters	$b = 20.536(21)$ Å	$\beta = 90°$
	$c = 7.7158(17)$ Å	$\gamma = 90°$
Volume	3632.35 Å^3	
Goodness-of-fit	5.179	

Figure S6. Variable temperature and pressure synchrotron X-ray powder diffraction data for **TIFSIX-4-Cu-i** in *d*-spacing (above) and *Q* (below).

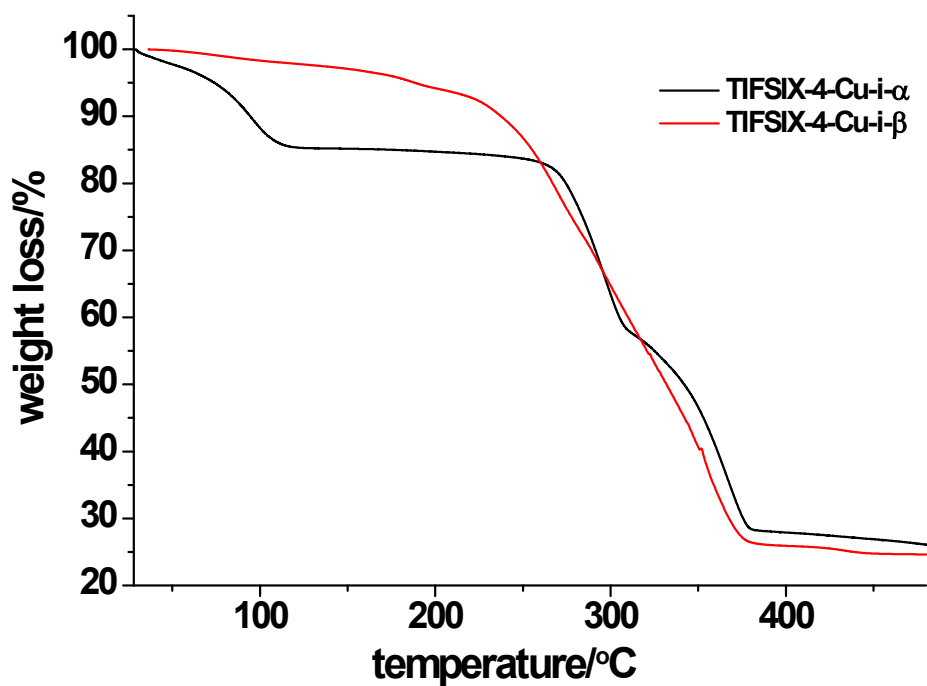## Thermogravimetric Analysis Data

Figure S7. TGA for **TIFSIX-4-Cu-i-α** and **TIFSIX-4-Cu-i-β**.
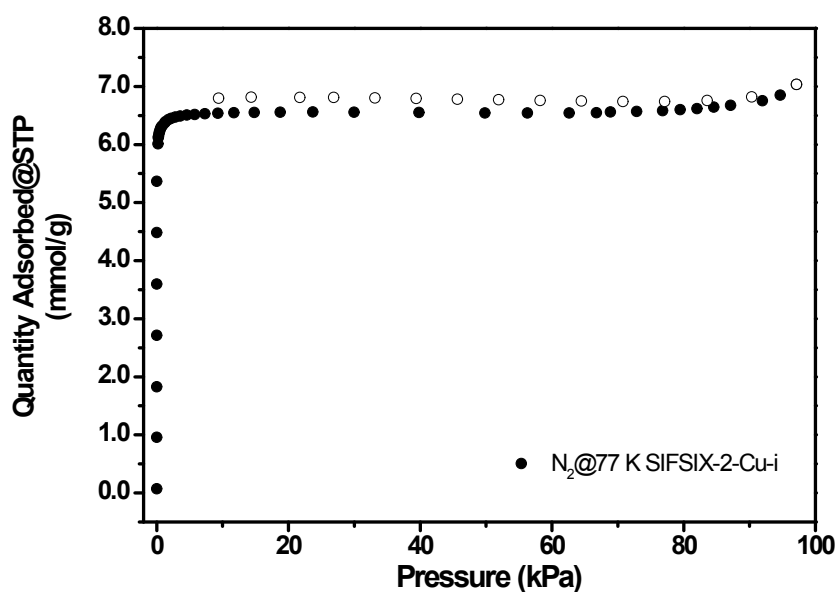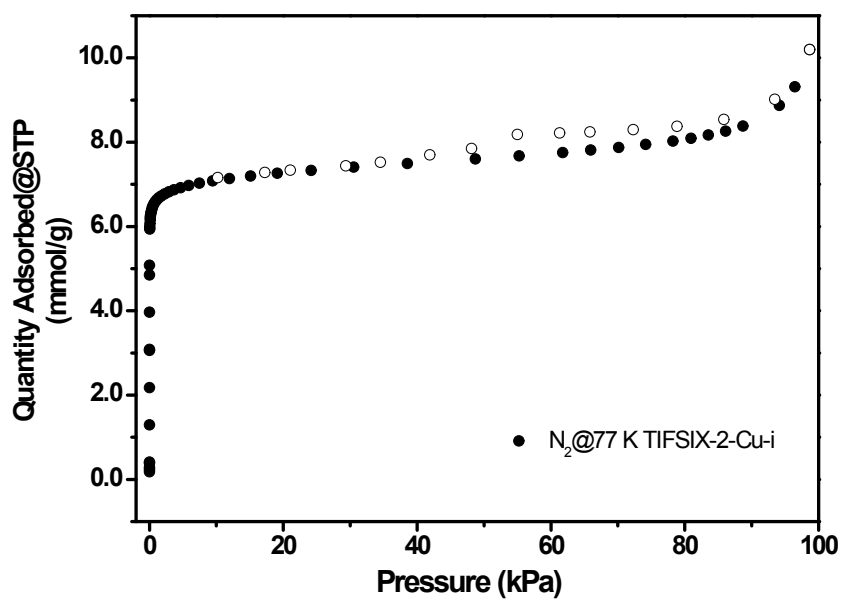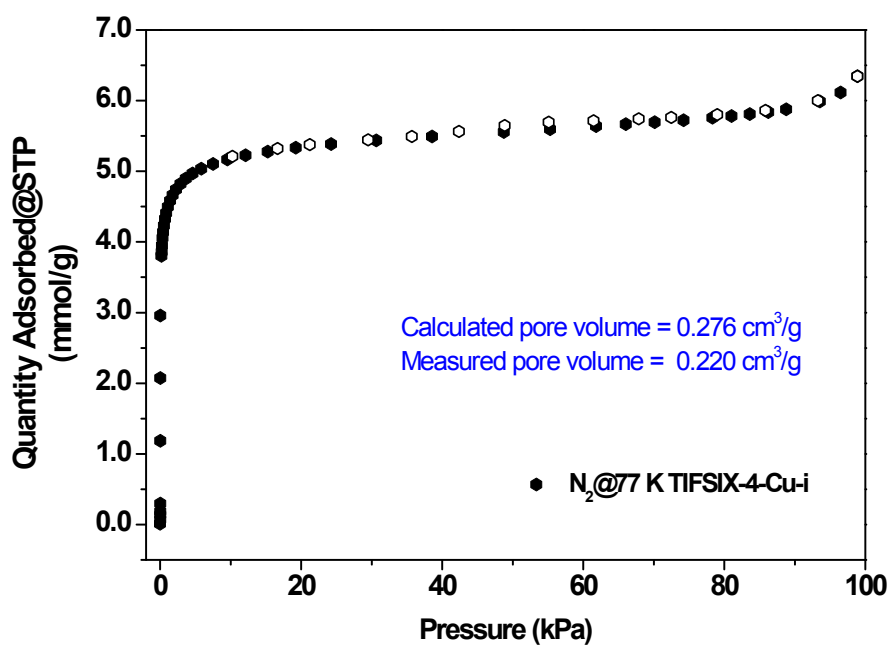
Low-Pressure Gas Adsorption Data

Figure S8. N_2 sorption data (solid symbols: adsorption; empty symbols: desorption) of **SIFSIX-2-Cu-i** at 77 K.

Figure S9. N$_2$ sorption data (solid symbols: adsorption; empty symbols: desorption) of **TIFSIX-2-Cu-i** at 77 K.

Figure S10. N$_2$ sorption data (solid symbols: adsorption; empty symbols: desorption) of **TIFSIX-4-Cu-i** at 77 K.
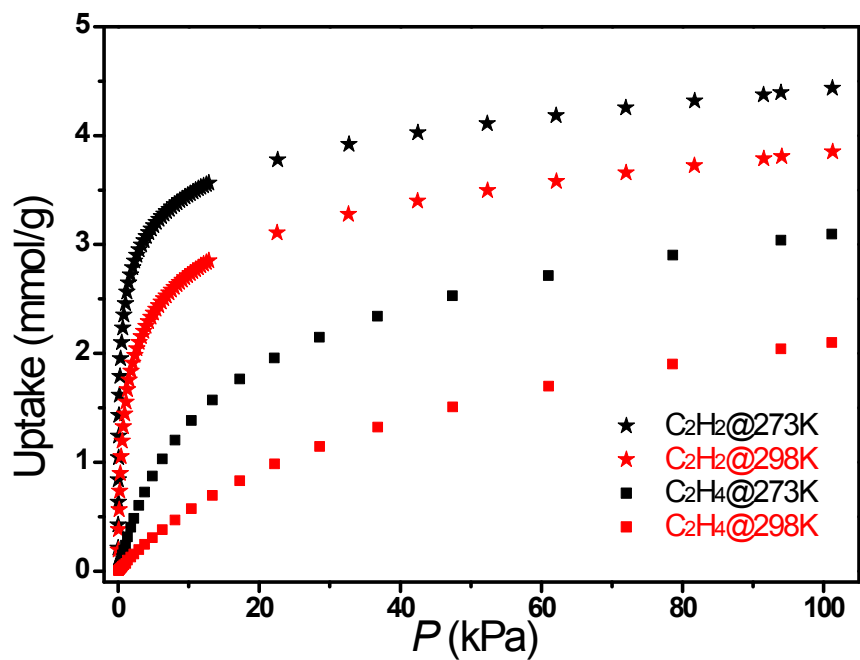
14

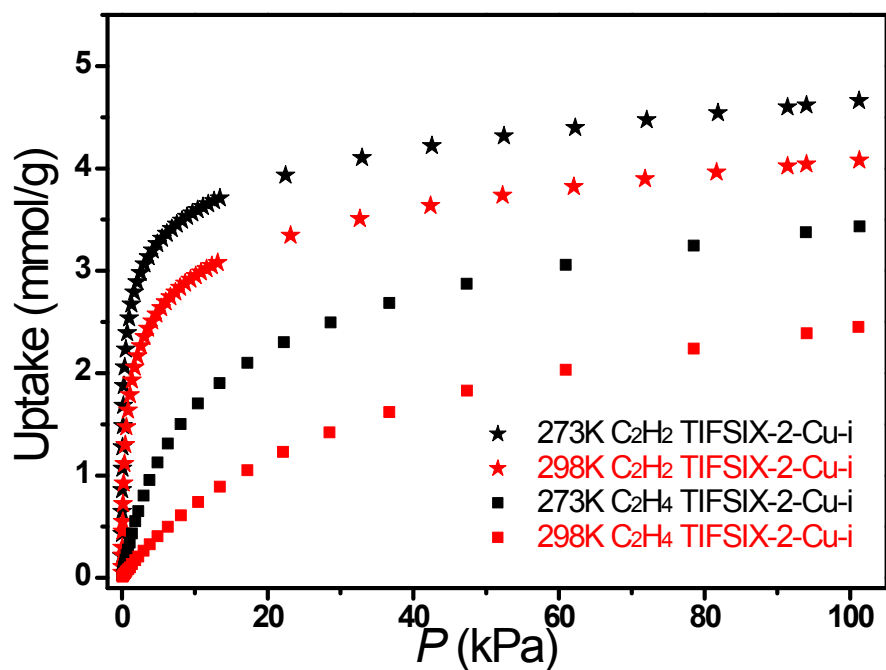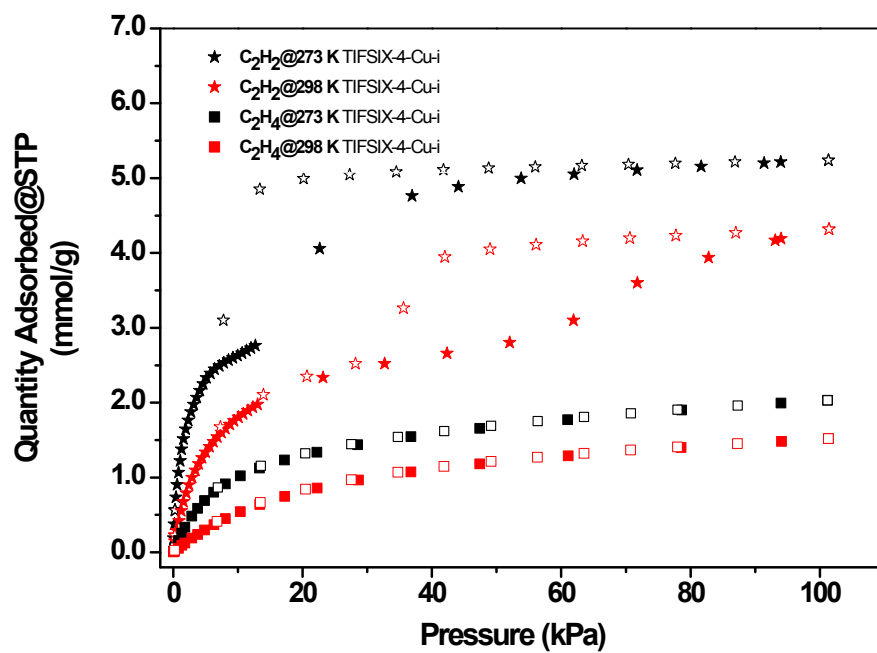**Figure S11.** C_2H_4 and C_2H_2 sorption data of **SIFSIX-2-Cu-i** at 273 and 298 K.

Figure S12. C_2H_4 and C_2H_2 sorption data of **TIFSIX-2-Cu-i** at 273 and 298 K.

Figure S13. C_2H_4 and C_2H_2 sorption data (solid symbols: adsorption; empty symbols: desorption) of **TIFSIX-4-Cu-i** at 273 and 298 K.
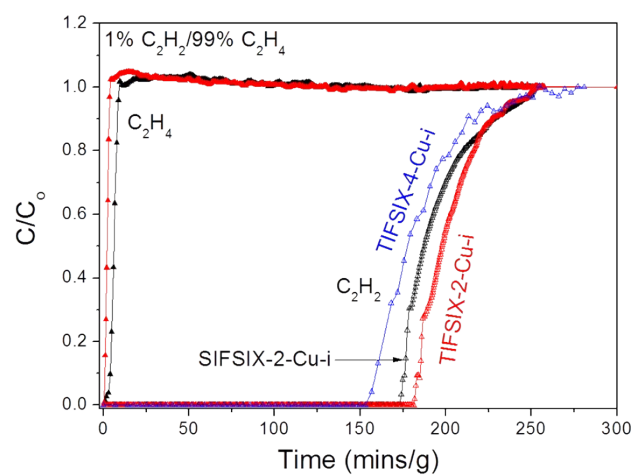
Dynamic Gas Breakthrough Measurement Data

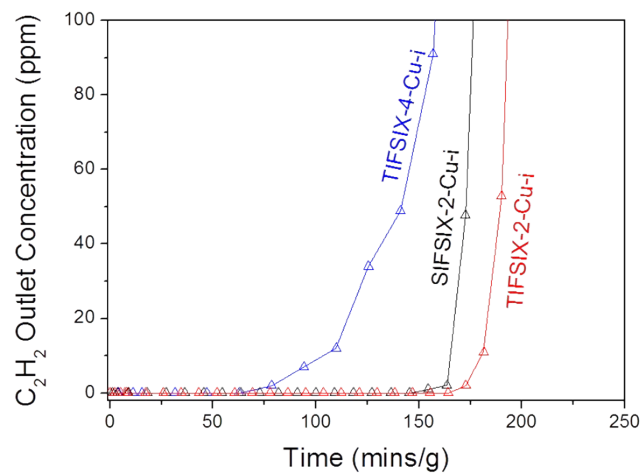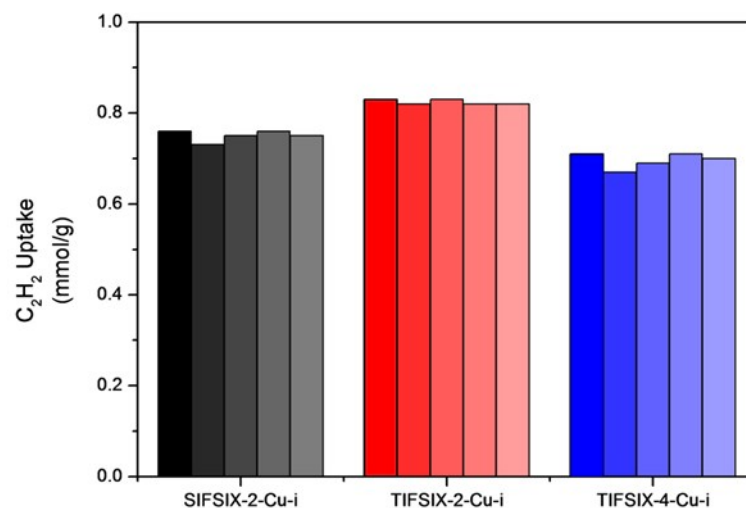**Figure S14.** 1:99 C_2H_2/C_2H_4 dynamic breakthrough curves 298 K.
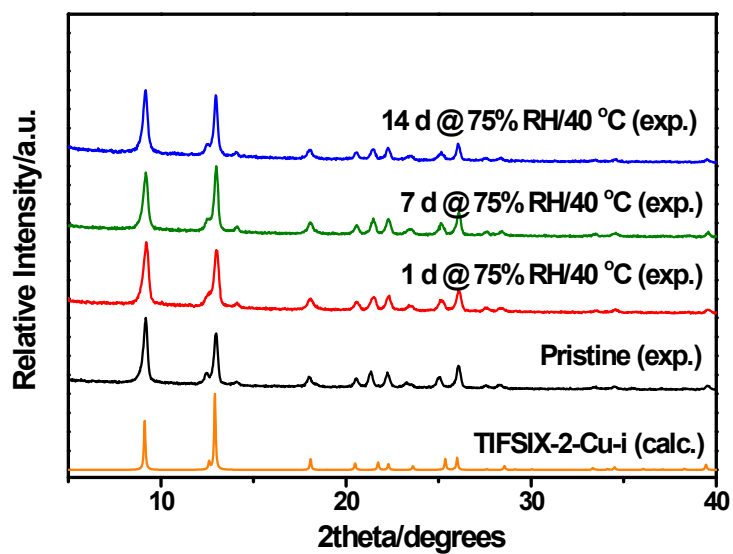

Figure S15. 1:99 C_2H_2/C_2H_4 dynamic breakthrough curves 298 K.

Figure S16. Results of recyclability experiments for HUMs when regeneration is carried out at 60 °C.

Accelerated Stability Data

Figure S17. PXRD patterns of **TIFSIX-2-Cu-i** after accelerated stability testing.
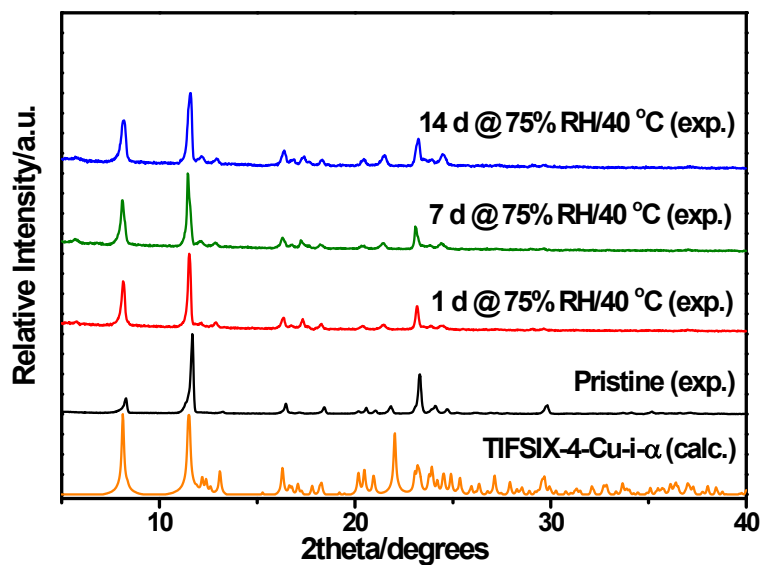
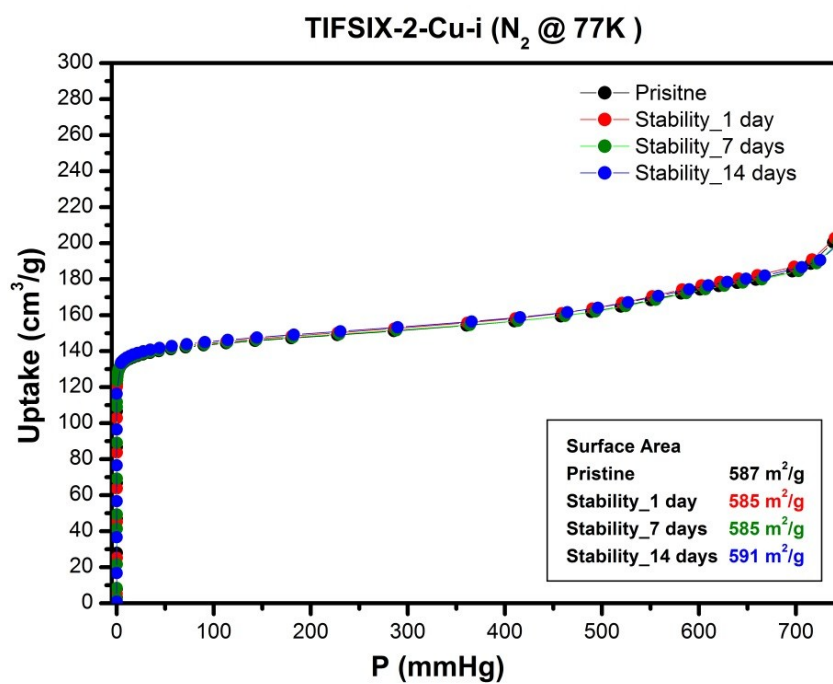**Figure S18.** PXRD patterns of **TIFSIX-4-Cu-i** after accelerated stability testing.

Figure S19. 77 K N_2 sorption data of **TIFSIX-2-Cu-i** after accelerated stability testing.
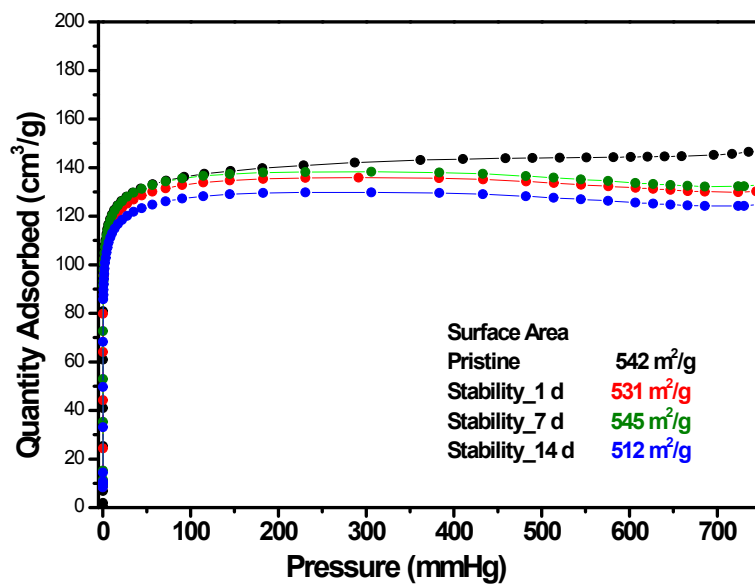
Figure S20. 77 K N$_2$ sorption data of **TIFSIX-4-Cu-i** after accelerated stability testing.

Calculations of Isosteric Enthalpies of Adsorption

$$lnP = lnN + \sum_{i=0}^{m} a_i N^i + \sum_{i=0}^{n} \binom{n}{k} b_i N^i$$

$$Q_{st} = -R \sum_{i=0}^{m} a_i N^i$$

A virial-type expression of the above form was used to fit the combined isotherm data for all these four compounds at 273 and 298 K, where P is the pressure described in Pa, N is the adsorbed amount in mmol/g, T is the temperature in K, a_i and b_i are virial coefficients, and m and n are the number of coefficients used to describe the isotherms. Q_{st} is the coverage-dependent enthalpy of adsorption and R is the universal gas constant. (**Figure S21-S26**).

Legend:
- ■ C_2H_2@273K
- ● C_2H_2@298K
- —— Fitting for 273K SIFSIX-2-Cu-i
- —— Fitting for 298K SIFSIX-2-Cu-i

Equation	y = ln(x)+1/T*(a0+a1*x+a2*x^2+a3*x^3+a4*x^4+a5*x^5)+(b0+b1*x+b2*x^2+b3*x^3)	
Adj. R-Square		0.99976
	Value	Standard Error
T	273	0
a0	-6340.87535	21.26347
a1	105.31255	9.69506
a2	89.06294	4.50508
a3	-4.33042	0.61797
b0	26.60077	0.07363
T	298	0

Figure S21. The virial fitting of C_2H_2 sorption data for **SIFSIX-2-Cu-i**.

Figure S22. The virial fitting of C_2H_4 sorption data for **SIFSIX-2-Cu-i**.
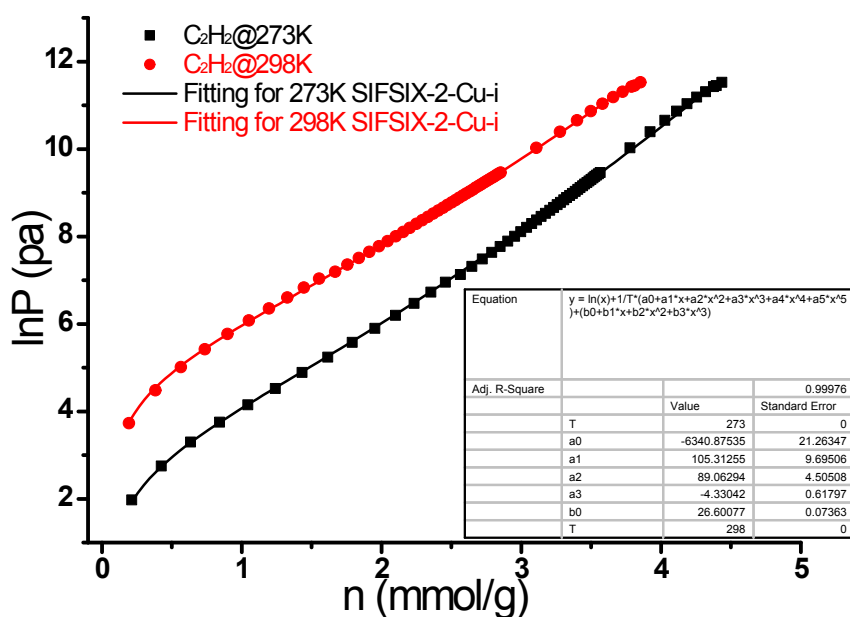

Figure S23. The virial fitting of C_2H_2 sorption data for **TIFSIX-2-Cu-i**.

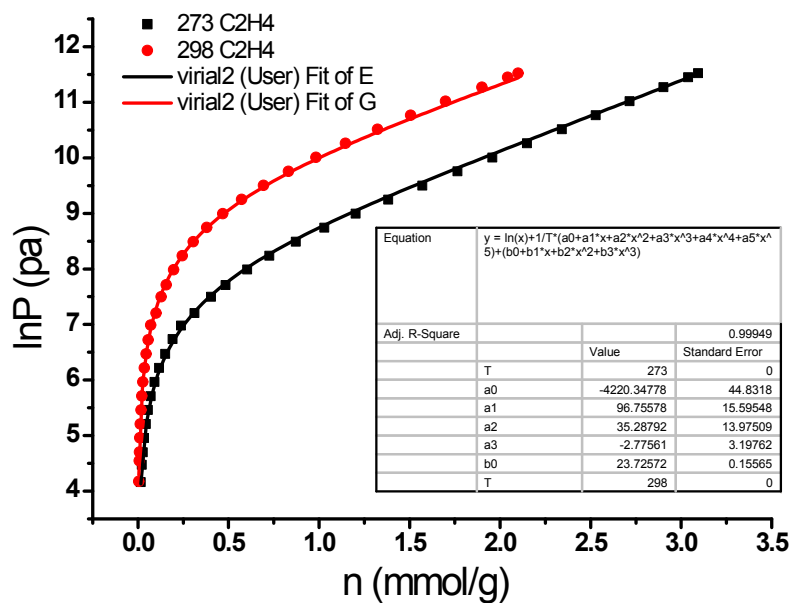**Figure S24.** The virial fitting of C_2H_4 sorption data for **TIFSIX-2-Cu-i**.
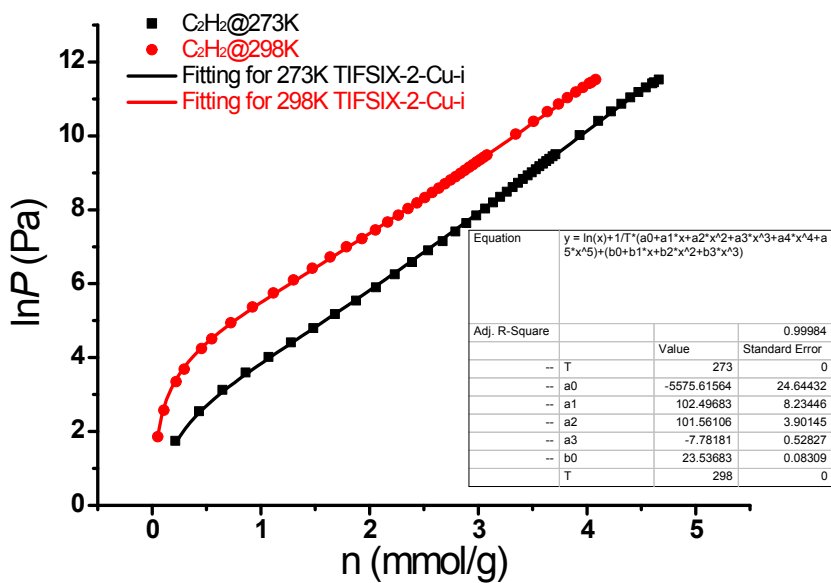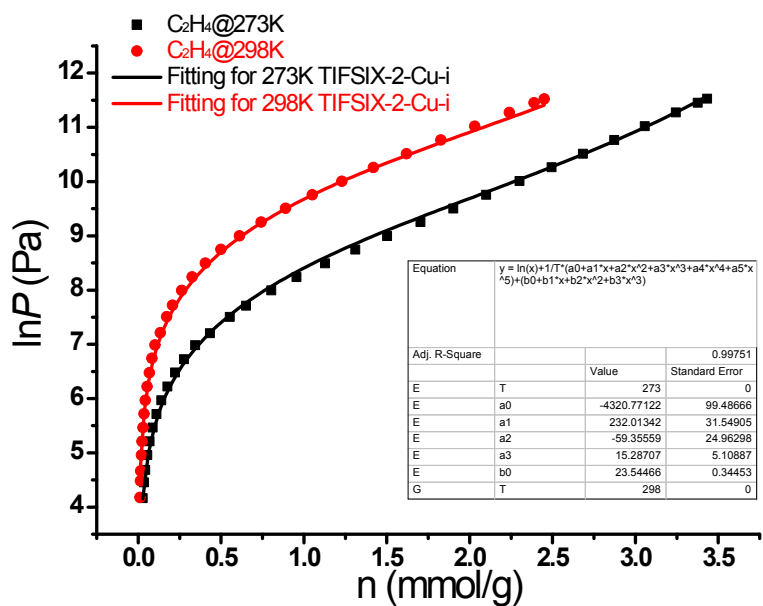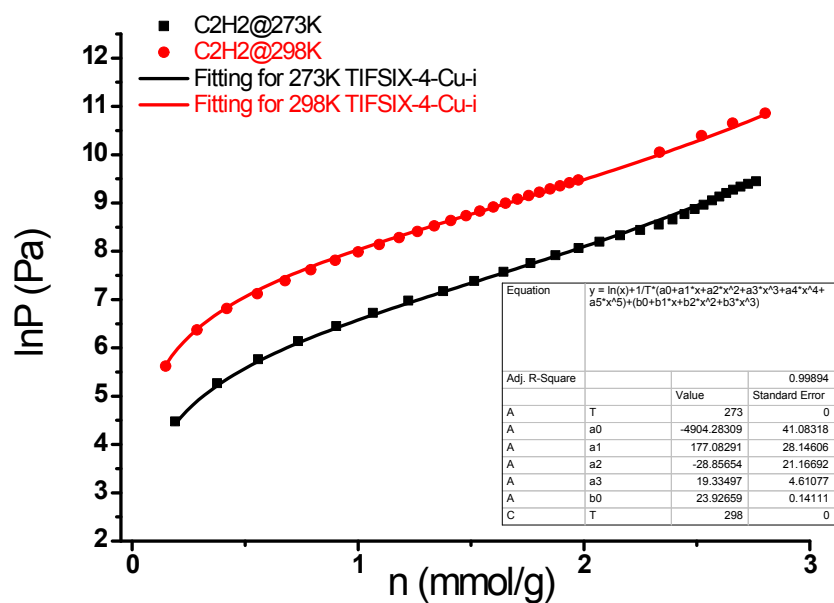

Figure S25. The virial fitting of C_2H_2 sorption data for **TIFSIX-4-Cu-i**.
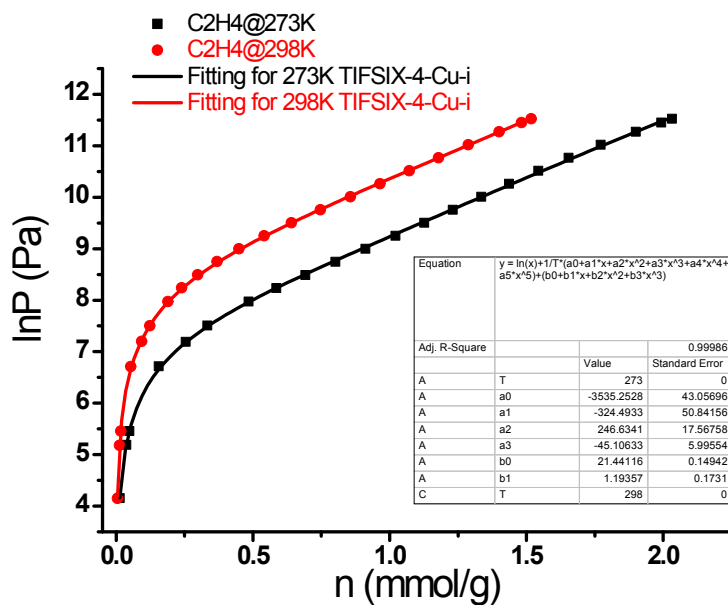
Figure S26. The virial fitting of C_2H_4 sorption data for **TIFSIX-4-Cu-i**.
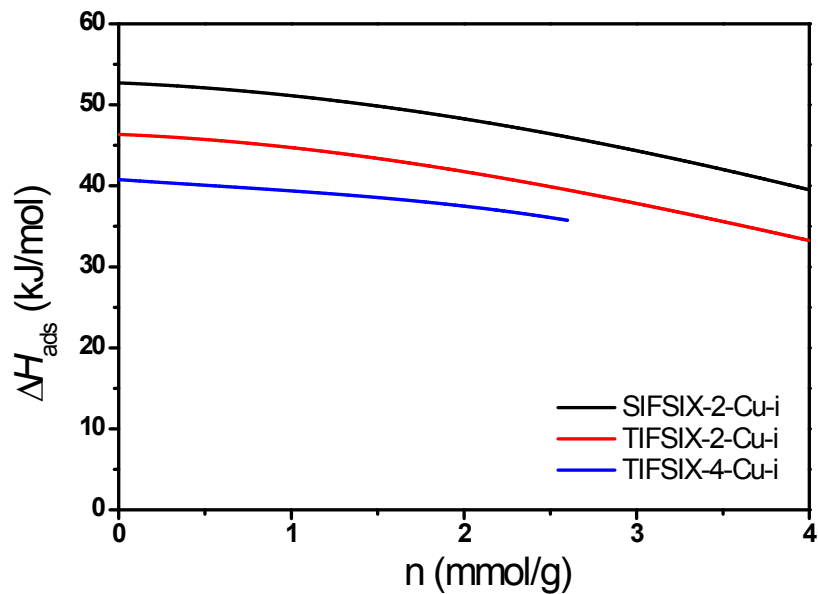

Figure S27. Isosteric heats of adsorption (Q_{st}) for C_2H_2 in **SIFSIX-2-Cu-i**, **TIFSIX-2-Cu-i**, **TIFSIX-4-Cu-i**.

Calculation of IAST Selectivities

The C_2H_2/C_2H_4 selectivities for the adsorbate mixture composition of interest (1:99) in **TIFSIX-2-Cu-i** and **TIFSIX-4-Cu-i** were predicted from the single-component adsorption isotherms using Ideal Adsorbed Solution Theory (IAST),[11] as employed in IAST++.[12] First, the single-component isotherms for the adsorbates at 298 K were fitted to the dual-site Langmuir-Freundlich equation (**Table S3-S6**):

$$n(P) = \frac{n_{m1}b_1 P^{\left(\frac{1}{t_1}\right)}}{1 + b_1 P^{\left(\frac{1}{t_1}\right)}} + \frac{n_{m2}b_2 P^{\left(\frac{1}{t_2}\right)}}{1 + b_2 P^{\left(\frac{1}{t_2}\right)}}$$

In this equation, n is the amount adsorbed per mass of material (in mmol g^{-1}), P is the total pressure (in kPa) of the bulk gas at equilibrium with the adsorbed phase, n_{m1} and n_{m2} are the saturation uptakes (in in mmol g^{-1}) for sites 1 and 2, b_1 and b_2 are the affinity coefficients (in kPa^{-1}) for sites 1 and 2, and t_1 and t_2 represent the deviations from the ideal homogeneous surface (unitless) for sites 1 and 2. The parameters that were obtained from the fitting for **TIFSIX-2-Cu-i** and **TIFSIX-4-Cu-i** are found in **Tables S2-S4**, respectively. All isotherms were fitted with R^2 > 0.999. Next, the spreading pressure for adsorbates i and j can be calculated using the following equations:

$$\frac{\pi^{\circ}_i A}{RT} = \int_0^{P^{\circ}_i(\pi)} \frac{n_i(P)}{P} dP$$

$$\frac{\pi^{\circ}_j A}{RT} = \int_0^{P^{\circ}_j(\pi)} \frac{n_j(P)}{P} dP$$

In the above equations, A represents the specific surface area (assumed to be the same for all adsorbates), R is the ideal gas constant, T is the temperature, and $P^{\circ}_i(\pi)$ and $P^{\circ}_j(\pi)$ are the equilibrium gas phase pressures corresponding to the solution temperature and solution spreading pressure for the adsorption of pure components i and j, respectively. Further, the following equations hold true for a two-component mixture according to IAST:

$$\pi^{\circ}_i = \pi^{\circ}_j$$

$$Py_i = P^{\circ}_i x_i$$

$$Py_i = P^{\circ}_{i}x_i$$

$$x_i + x_j = 1$$

$$y_i + y_j = 1$$

Here, x_i and x_j are the mole fractions of components i and j, respectively, in the adsorbed phase, and y_i and y_j are the mole fractions of components i and j, respectively, in the gas phase. The previous seven equations are seven independent equations with nine unknowns. In order to solve for all of the unknowns, two quantities must be specified, particularly P and y_i. Utilisation of the aforementioned equations yields the following equilibrium expression for adsorbates i and j:

$$\int_0^{\frac{Py_i}{x_i}} \frac{n_i(P)}{P}\,dP = \int_0^{\frac{P(1-y_i)}{(1-x_i)}} \frac{n_j(P)}{P}\,dP$$

The above equation was solved for x_i using numerical analysis[3] for a range of pressures at a specified y_i value. Finally, the selectivity for adsorbate i relative to adsorbate j was calculated using the following:

$$S_{i/j} = \frac{x_i y_j}{x_j y_i}$$

Table S3. The fitted parameters for the dual-site Langmuir-Freundlich equation for the single-component isotherms of C_2H_2 and C_2H_4 in **SIFSIX-2-Cu-i** at 298 K. The R^2 value is also provided.

SIFSIX-2-Cu-i	C_2H_2	C_2H_4
q1	1.839770	3.211270
n2	0.636193	6.264300
k1	1.954210	0.018892
k2	0.038124	0.540229
n1	0.915876	0.944601
q2	2.824110	0.000000
R^2	0.999969	0.999943

Table S4. The fitted parameters for the dual-site Langmuir-Freundlich equation for the single-component isotherms of C_2H_2 and C_2H_4 in **TIFSIX-2-Cu-i** at 298 K. The R^2 value is also provided.

TIFSIX-2-Cu-i	C_2H_2	C_2H_4
q1	1.969370	3.410300
n2	0.650795	6.707000
k1	2.949600	0.024563
k2	0.044395	0.011037
n1	0.901259	0.943404
q2	2.868060	0.079916
R^2	0.999965	0.999995

Table S5. The fitted parameters for the dual-site Langmuir-Freundlich equation for the single-component isotherms of C_2H_2 and C_2H_4 in **TIFSIX-4-Cu-i** at 298 K. The R^2 value is also provided.
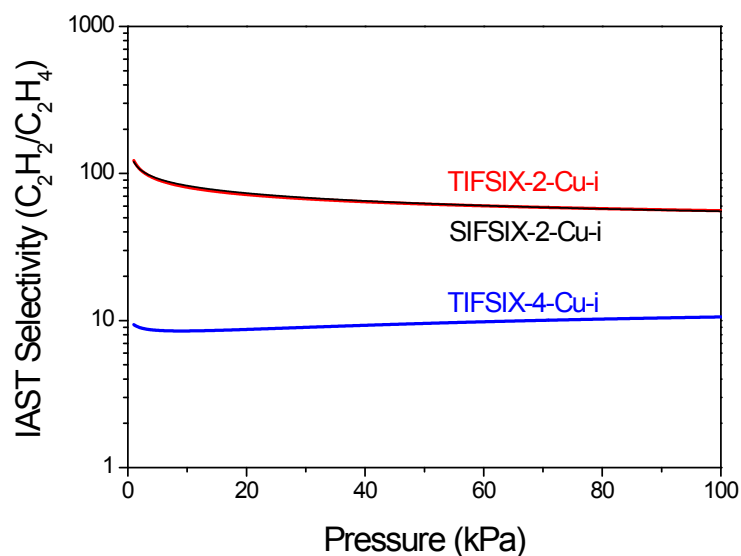
| TIFSIX-4-Cu-i	C_2H_2	C_2H_4
q1	2.794214	1.919930
n2	0.199000	2.092760
k1	1.044462	0.035741
k2	0.268247	1.755400
n1	0.000000	0.968315
q2	2.531765	0.000000
R^2	0.999033	0.999822

Figure S28. IAST selectivities for 1/99 C_2H_2/C_2H_4 gas mixtures for **SIFSIX-2-Cu-i**, **TIFSIX-2-Cu-i**, **TIFSIX-4-Cu-i** at 298 K.

Molecular Modelling

The point partial charges for the chemically distinct atoms in **SIFSIX-2-Cu-i** and **TIFSIX-2-Cu-i** (**Figure S29**) were determined through electronic structure calculations on different representational fragments that were selected from the crystal structure of the respective HUMs as implemented previously.[13,14] The resulting partial charges for each unique atom in both HUMs are shown in **Table S6**.
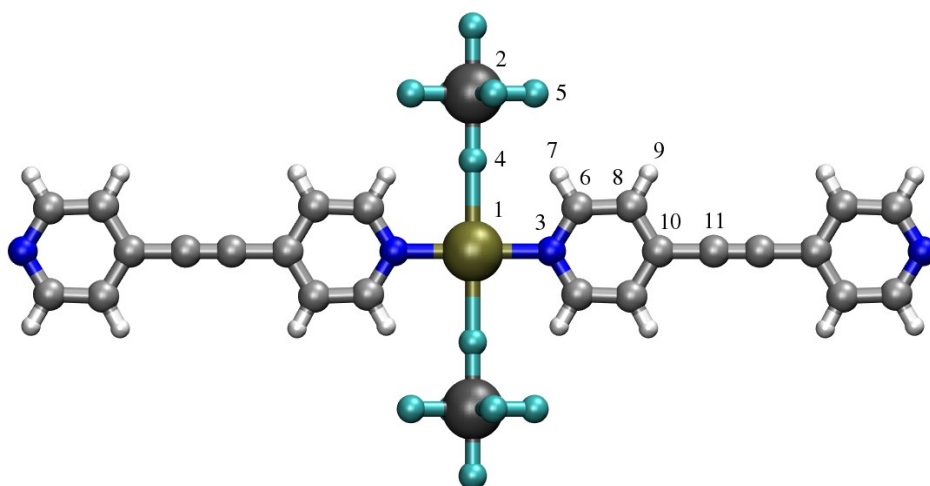
Figure S29. The numbering of the chemically distinct atoms in **SIFSIX-2-Cu-i** and **TIFSIX-2-Cu-i** as referred to in **Table S6**. C = light gray, H = white, N = blue, F = cyan, Si/Ti = dark gray, Cu = gold.

Table S6. Calculated partial charges (in e^-) for the chemically distinct atoms in **SIFSIX-2-Cu-i** and **TIFSIX-2-Cu-i**. Label of atoms correspond to **Figure S29**. The yellow highlight indicates the atom that will have the most interactions with the adsorbate.

Atom	Label	SIFSIX-2-Cu-i	TIFSIX-2-Cu-i
Cu	1	0.2893	0.9609
Si/Ti	2	1.5887	1.7253
N	3	−0.0572	−0.2953
F	4	−0.5342	−0.4561
F	5	−0.5627	−0.6309
C	6	0.1451	0.1636
H	7	0.1580	0.1604
C	8	−0.3209	−0.3876
H	9	0.1781	0.1876
C	10	0.2539	0.3647
C	11	−0.1570	−0.1300

(a)   (b)
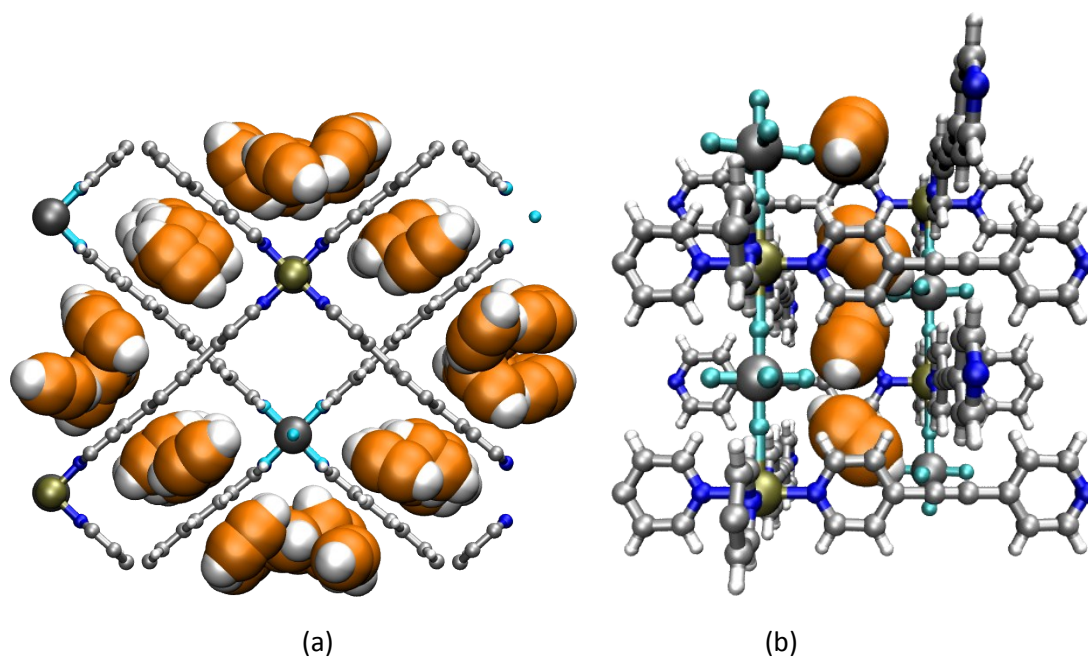
Figure S30. (a) Orthographic c-axis view of the $1 \times 1 \times 3$ supercell of **TIFSIX-4-Cu-i** showing C_2H_2 molecules adsorbed within the channels of the HUM according to molecular simulations. (b) Perspective a/b-axis view of a portion of the crystal structure of **M'FSIX-2-Cu-i (M' = Si, Ti)** showing C_2H_2 molecules localized within the channels of the HUM according to molecular simulations. C(HUM) = light gray, C(C_2H_2) = orange, H = white, N = blue, F = cyan, Si/Ti = dark gray, Cu = gold.

References

1. Bajpai, A.; Scott, H. S.; Pham, T.; Chen, K.-J.; Space, B.; Lusi, M.; Perry, M. L.; Zaworotko, M. J.; *IUCrJ,* **2016**, 3. 430-439.

2. Kumar, A.; Hua, C.; Madden, D. G.; O'Nolan, D.; Chen, K.-J.; Keane, L.-A.; Perry IV, J. J.; Zaworotko, M. J. *Chem. Commun.,* **2017**, DOI: 10.1039/C7CC02289A.

3. (a) Nugent, P.' Belmabkhout, Y.; Adil, K.; Bhatt, P. M.; Cairns, A. J.; Eddaoudi, M.; Zaworotko, M. J. *Nature,* **2013**, 495, 80-84. (b) Cui, X.; Chen, K.-J.; Xing, H.; Yang, Q.; Krishna, R.; Bao, Z.; Wu, H.; Zhou, W.; Dong, X.; Han, Y.; Li, B.; Ren, Q.; Zaworotko, M. J.; Chen, B. *Science,* **2016**, 353, 141. (c) Chen, K.-J.; Scott, H. S.; Madden, D. G.; Pham, T.; Kumar, A.; Bajpai, A.; Lusi, M.; Forrest, K. A.; Space, B.; Perry IV, J. J.; Zaworotko, M. J. *Chem,* **2016**, 1, 753.

4. Barbour, L. J. J. *Supramol. Chem.,* **2001**, 1, 189-191.

5. Tang, C. C.; Thompson, S. P.; Hill, T. P.; Wilkin, G. R.; Wagner, U. H. *Z. Kristall.,* **2007**, 26, 153-158.

6. Boultif, A.; Louer, D. *J. Appl. Cryst.,* **2004**, 37, 724-731.

7. David, W. I. F.; Shankland, K.; van de Streek, J.; Pidcock, E.; Motherwell, W. D. S.; Cole, J. C. *J. Appl. Cryst.,* **2006**, 39, 910-915.

8. Toby, B. H.; Von Dreele, R. *J. Appl. Cryst.,* **2013**, 46, 544-549.

9. Allen, F. H. *Acta Crystallogr. Sect. B-Struct. Sci.* **2002**, *58*, 380.

10. Allen, F. H.; Kennard, O. *Chem. Des. Automat. News* **1993**, *8*, 31.

11. Myers, A. L.; Prausnitz, J. M. *AIChE J.,* **1965**, 11, 121-127.

12. Lee, S. IAST++ Official Homepage. https://sites.google.com/site/iastcpp/ (accessed Jun. 11, 2017).

13. T. Pham, K. A. Forrest, K. McLaughlin, B. Tudor, P. Nugent, A. Hogan, A. Mullen, C. R. Cioce, M. J. Zaworotko and B. Space, *J. Phys. Chem. C,* **2013**, 117, 9970–9982.

14. K.-J. Chen, H. S. Scott, D. G. Madden, T. Pham, A. Kumar, A. Bajpai, M. Lusi, K. A. Forrest, B. Space, J. J. Perry IV and M. J. Zaworotko, *Chem,* **2016**, 1, 753–765.